Anal. Chem. **2008,** *80,* 4575–4582

Accelerated Articles

Ambient Molecular Imaging and Depth Profiling of Live Tissue by Infrared Laser Ablation Electrospray Ionization Mass Spectrometry

Peter Nemes, Alexis A. Barton, Yue Li, and Akos Vertes*

Department of Chemistry, W. M. Keck Institute for Proteomics Technology and Applications, George Washington University, Washington, D.C. 20052

Mass spectrometry in conjunction with atmospheric pressure ionization methods enables the in vivo investigation of biochemical changes with high specificity and sensitivity. Laser ablation electrospray ionization (LAESI) is a recently introduced ambient ionization method suited for the analysis of biological samples with sufficient water content. With LAESI mass spectrometric analysis of chimeric *Aphelandra squarrosa* leaf tissue, we identify the metabolites characteristic for the green and yellow sectors of variegation. Significant parts of the related biosynthetic pathways (e.g., kaempferol biosynthesis) are ascertained from the detected metabolites and metabolomic databases. Scanning electron microscopy of the ablated areas indicates the feasibility of both two-dimensional imaging and depth profiling with a ~350 μm lateral and ~50 μm depth resolution. Molecular distributions of some endogenous metabolites show chemical contrast between the sectors of variegation and quantitative changes as the ablation reaches the epidermal and mesophyll layers. Our results demonstrate that LAESI mass spectrometry opens a new way for ambient molecular imaging and depth profiling of metabolites in biological tissues and live organisms.

In the past two decades, mass spectrometry (MS) has provided dramatic new insight into biological processes. The key factor that has enabled these advances is our ability to ionize and identify a wide range of molecular classes with high accuracy, excellent selectivity, and low detection limits. Electrospray ionization (ESI) and matrix-assisted laser desorption/ionization (MALDI) have brought peptides, proteins, their noncovalent complexes, and other biomolecular classes within the reach of detailed mass spectrometric investigations.[1] While ESI calls for solution-phase samples of specific conductivity, MALDI requires the presence of a denaturing matrix and operates in vacuum. These conditions are incompatible with in vivo investigations. Consequently, there is a need for methods that achieve efficient ion generation under nativelike experimental conditions.

Technical innovations of recent years have provided an arsenal of ambient ion sources[2] for MS. Many of them apply physical or chemical pretreatments or conditions that are known to disrupt living organisms; thus, the choice of techniques suitable for in vivo MS narrows down to a few. For example, desorption electrospray ionization has been applied successfully for the detection of drugs, metabolites, and explosives on human fingers,[3,4] on untreated *Escherichia coli*, and on different strains of *Salmonella typhimurium* cells.[5] Most recently, DESI-mass spectral fingerprints have allowed rapid biodetection for a variety of bacteria.[6] MALDESI,[7] a combination of MALDI and DESI, has enabled the characterization of intact polypeptides.[8] Human breath and fruit maturity have been investigated by extractive electrospray ionization.[9,10] Atmospheric pressure infrared MALDI (AP IR-MALDI),[11,12] electrospray-assisted laser desorption/ionization (ELDI),[13] and laser ablation electrospray ionization (LAESI)[14] employ focused laser radiation for ambient sampling. AP IR-MALDI and LAESI have proved particularly useful in targeting primary and secondary plant metabolites with no sample preparation or chemical modification required. Following the introduction

* To whom correspondence should be addressed. E-mail: vertes@gwu.edu. Phone: (202) 994-2717. Fax: (202) 994-5873

(1) Siuzdak, G. *Proc. Natl. Acad. Sci. U. S. A.* **1994**, *91*, 11290–11297.
(2) Cooks, R. G.; Ouyang, Z.; Takats, Z.; Wiseman, J. M. *Science* **2006**, *311*, 1566–1570.
(3) Takats, Z.; Wiseman, J. M.; Gologan, B.; Cooks, R. G. *Science* **2004**, *306*, 471–473.
(4) Justes, D. R.; Talaty, N.; Cotte-Rodriguez, I.; Cooks, R. G. *Chem. Commun.* **2007**, 2142–2144.
(5) Song, Y. S.; Talaty, N.; Tao, W. A.; Pan, Z. Z.; Cooks, R. G. *Chem. Commun.* **2007**, 61–63.
(6) Meetani, M. A.; Shin, Y. S.; Zhang, S. F.; Mayer, R.; Basile, F. *J. Mass Spectrom.* **2007**, *42*, 1186–1193.
(7) Sampson, J. S.; Hawkridge, A. M.; Muddiman, D. C. *J. Am. Soc. Mass Spectrom.* **2006**, *17*, 1712–1716.
(8) Sampson, J. S.; Hawkridge, A. M.; Muddiman, D. C. *Rapid Commun. Mass Spectrom.* **2007**, *21*, 1150–1154.
(9) Chen, H. W.; Wortmann, A.; Zhang, W. H.; Zenobi, R. *Angew. Chem., Int. Ed.* **2007**, *46*, 580–583.
(10) Chen, H. W.; Sun, Y. P.; Wortmann, A.; Gu, H. W.; Zenobi, R. *Anal. Chem.* **2007**, *79*, 1447–1455.
(11) Li, Y.; Shrestha, B.; Vertes, A. *Anal. Chem.* **2007**, *79*, 523–532.
(12) Li, Y.; Shrestha, B.; Vertes, A. *Anal. Chem.* **2008**, *80*, 407–420.
(13) Shiea, J.; Huang, M. Z.; Hsu, H. J.; Lee, C. Y.; Yuan, C. H.; Beech, I.; Sunner, J. *Rapid Commun. Mass Spectrom.* **2005**, *19*, 3701–3704.
(14) Nemes, P.; Vertes, A. *Anal. Chem.* **2007**, *79*, 8098–8106.

10.1021/ac8004082 CCC: $40.75
Published on Web 05/13/2008

of LAESI,[14] a similar arrangement was proposed and termed infrared laser-assisted desorption electrospray ionization.[15]

DESI and LAESI offer some unique advantages in several respects. Their common feature, attachment of multiple charges to the analyte molecules through electrostatic spraying, extends the analyzable mass range up to a neutral mass of ~66 kDa. This is coupled with a ~5-decade dynamic range in quantitation and limits of detection down to a few femtomoles.[14,16] These figures of merits have enabled in vivo biochemical analyses by DESI and LAESI.

The spatial distributions of biomolecules in tissues and organs can be revealing for the understanding of underlying biochemical and physiological processes. Imaging molecular mass spectrometry under vacuum conditions through both secondary ion MS (SIMS) and MALDI has already shown its potential for recovering drug and metabolite distributions in tissue or whole-body sections.[17–19] Similar capabilities are being developed for the ambient environment. AP IR-MALDI and DESI have demonstrated success in this endeavor by following metabolite transport induced by the transpirational pull in plant vasculature and by routinely imaging a rat brain section, respectively.[20–22] Spatial resolution of these methods can be estimated at ~200−300 μm. This can further be improved by tighter focusing of the incident laser beam or by oversampling in AP IR-MALDI imaging.[11] For the DESI methodology decreased solution supply rates, smaller emitter dimensions (e.g., nanoelectrospray) and the proper selection of nebulizing gas velocity and scan direction[21,23–25] has shown improvements.

The low ionization yields reported for UV-MALDI[26–28] and the decreased photon energies and absorption coefficients in the mid-infrared region indicate that the ablation plume produced in AP IR-MALDI mostly consists of uncharged molecules, clusters, and particulates. Whereas IR-MALDI aims at the direct detection of this rather small ionic fraction, LAESI and ELDI offer a significant improvement by postionizing the neutrals in the laser plume using the charged droplets from of an electrospray.

LAESI and ELDI might show similarities on the surface, i.e., both rely on the postionization of neutrals in a laser plume by ESI, but these two techniques exhibit some fundamental differences. Due to the strong absorption of 2.94-μm light by water molecules, the coupling of laser energy to water-rich targets in LAESI is a resonant process. In contrast ELDI uses UV light to produce off-resonance laser ablation of the sample. As a consequence, biomolecules such as peptides, proteins, and DNA are directly exposed to UV irradiation with a possibility for photochemical dissociation of chemical bonds.[29] In ELDI, some of the absorbed energy is converted into vibrational excitation of the sample molecules leading to photothermal ablation. In contrast, in the mid-infrared region of the spectrum, photochemical processes are negligible; the prevailing chromophore in LAESI is water. LAESI relies on recoil-induced material expulsion to deliver intact sample particulates into the electrospray for postionization. As a consequence, the range of samples and the analytical figures of merit are very different for LAESI and ELDI.

In this contribution, we show for the first time that the local sampling capability of LAESI can be exploited for molecular imaging. We introduce LAESI-MS imaging, and apply the method to follow the spatial distributions of metabolites in live Zebra plant (*Aphelandra squarrosa*) leaves. This chimeric organ has light yellow stripes on its surface that run adjacent to the primary and secondary veins. The molecular images produced by LAESI in combination with optical and scanning electron microscopy allow us to identify metabolic pathways specific to the variegation. As consecutive laser shots to the same point ablate increasingly deeper layers of the tissue, depth profiling of the metabolites is achieved. Our results demonstrate the feasibility of LAESI-MS for two-dimensional molecular imaging and for depth profiling, for the investigation of biochemical changes in live organisms.

EXPERIMENTAL SECTION

Laser Ablation Electrospray Ionization. The electrospray system was identical to the one described in our recent study.[14] Briefly, 50% methanol solution containing 0.1% (v/v) acetic was fed through a tapered tip metal emitter (100-μm i.d. and 320-μm o.d., New Objective, Woburn, MA) using a low-noise syringe pump (Physio 22, Harvard Apparatus, Holliston, MA). Stable high voltage was directly applied to the emitter by a regulated power supply (PS350, Stanford Research System, Inc., Sunnyvale, CA). The flow rate and the spray voltage were adjusted to establish the cone-jet regime. This axial spraying mode has been reported to be the most efficient for ion production.[30,31] Approximately 15×15 mm^2 area of a Zebra plant leaf was mounted on a microscope slide, positioned 18 mm below the spray axis. A Nd:YAG laser was operated at a 10-Hz repetition rate (4-ns pulse duration), and the output was converted to 2940 nm via an optical parametric oscillator (Vibrant IR, Opotek Inc., Carlsbad, CA). This mid-infrared laser beam was focused with a plano-convex focusing lens (50-mm focal length) and was used to ablate the leaf samples at 90° incidence angle, ~5−8 mm downstream from the tip of the spray emitter. Using optical microscopy, the ablated area was determined to be circular and ~350 μm in diameter. The material removal was further characterized by imaging the craters with scanning electron microscopy (JEOL JSM-840A, Peabody, MA). During the *A. squarrosa* imaging experiments, the average output energy of a laser pulse was measured to be 2.0 mJ with 7% stability,

(15) Rezenom, Y. H.; Dong, J.; Murray, K. K. *Analyst* **2008**, *133*, 226–232.
(16) Takats, Z.; Wiseman, J. M.; Cooks, R. G. *J. Mass Spectrom.* **2005**, *40*, 1261–1275.
(17) Khatib-Shahidi, S.; Andersson, M.; Herman, J. L.; Gillespie, T. A.; Caprioli, R. M. *Anal. Chem.* **2006**, *78*, 6448–6456.
(18) McDonnell, L. A.; Heeren, R. M. A. *Mass Spectrom. Rev.* **2007**, *26*, 606–643.
(19) Ostrowski, S. G.; Van Bell, C. T.; Winograd, N.; Ewing, A. G. *Science* **2004**, *305*, 71–73.
(20) Li, Y.; Shrestha, B.; Vertes, A. *Anal. Chem.* **2007**, *80*, 407–420.
(21) Ifa, D. R.; Wiseman, J. M.; Song, Q. Y.; Cooks, R. G. *Int. J. Mass Spectrom.* **2007**, *259*, 8–15.
(22) Wiseman, J. M.; Ifa, D. R.; Cooks, R. G.; Venter, A. *Nat. Protocols* **2008**, *3*, 517–524.
(23) Wiseman, J. M.; Ifa, D. R.; Song, Q. Y.; Cooks, R. G. *Angew. Chem., Int. Ed.* **2006**, *45*, 7188–7192.
(24) Pasilis, S. P.; Kertesz, V.; Van Berkel, G. J. *Anal. Chem.* **2007**, *79*, 5956–5962.
(25) Kertesz, V.; Van Berkel, G. J. *Anal. Chem.* **2008**, *80*, 1027–1032.
(26) Ens, W.; Mao, Y.; Mayer, F.; Standing, K. G. *Rapid Commun. Mass Spectrom.* **1991**, *5*, 117–123.
(27) Mowry, C. D.; Johnston, M. V. *Rapid Commun. Mass Spectrom.* **1993**, *7*, 569–575.
(28) Puretzky, A. A.; Geohegan, D. B. *Chem. Phys. Lett.* **1998**, *286*, 425–432.
(29) Vogel, A.; Venugopalan, V. *Chem. Rev.* **2003**, *103*, 577–644.
(30) Valaskovic, G. A.; Kelleher, N. L.; Little, D. P.; Aaserud, D. J.; McLafferty, F. W. *Anal. Chem.* **1995**, *67*, 3802–3805.
(31) Nemes, P.; Marginean, I.; Vertes, A. *Anal. Chem.* **2007**, *79*, 3105–3116.

which translated into a fluence of 1.9−2.2 J/cm^2 at the focal point. The ablated material was intercepted by the electrospray plume. Ions generated during the LAESI process were mass analyzed by an orthogonal acceleration time-of-flight mass spectrometer (Q-TOF Premier, Waters Co., Milford, MA) with a 1 s/spectrum integration time. The original electrospray ion source of the mass spectrometer was removed. The sampling cone of the mass spectrometer was located on axis with and 13 mm away from the tip of the spray emitter. The ion optics settings of the instrument were optimized for best performance and were kept constant during the experiments. Metabolite identification was facilitated by tandem mass spectrometry. Fragmentation was induced by collision-activated dissociation in argon collision gas at 4×10^{-3} mbar pressure with the collision energy set between 15−30 eV.

Molecular Imaging with LAESI. A three-axis precision flexure stage (NanoMax TS, Thorlabs, Newton, NJ) was computer controlled to scan the sample surface, while keeping all other components of the LAESI setup in place. The flexure stage had a travel range of 4 mm and due to the piezoelectric actuators and displacement sensors an ultimate resolution of 25 nm. Thus, the spatial resolution of the imaging experiment was limited by the focal spot size of the laser beam and by the resulting ablation area (350-μm circle in diameter). To avoid the overlapping of the probed areas, the sample surface was scanned at a step size of 400 μm in the *X* and *Y* directions. At each position, the ions were collected for 10 s, yielding a total scan time of ∼20 min for a 16-mm^2 area, i.e., ∼1 h for the 48-mm^2 surface. In other experiments, the dwell time was set to 4 s while still maintaining an acceptable pixel-to-pixel separation in time (no or minimal cross talk). This enabled the total analysis time to be decreased by 60%, resulting in a 25-min data acquisition time for the 48-mm^2 surface area. For each pixel, the mass spectra were stored as a function of time. Our data acquisition program (written in LabVIEW 8.0) rendered the analysis times to the corresponding *X*−*Y* coordinates and converted these data sets into two-dimensional distributions. A scientific visualization package (Origin 7.0, OriginLab Co., Northampton, MA) was used to produce contour plot images for the distributions of mass-selected ions.

Chemicals. The electrosprayed solutions were prepared using glacial acetic acid (TraceSelect grade) and gradient grade methanol and water solvents. All chemicals were obtained from Sigma-Aldrich and were used as received. The Zebra plant (*A. squarrosa*) and the Easter lily (*Spathiphyllum lynise*) were purchased from a local florist at an approximate age of one year. The plants were watered every 2 days with ∼300 mL of tap water to keep their soil moderately moist to touch. No fertilizer was used during the experiments. Temperature and light conditions were 20−25 °C in light shade, protected from direct sun.

RESULTS AND DISCUSSION

Midinfrared Laser Ablation of Leaf Tissue. Optical microscopy of the *A. squarrosa* leaves after LAESI-MS analysis indicated increasing tissue removal with consecutive laser pulses. This was consistent with reports showing that mid-infrared ($\lambda = 2.94$ μm) laser ablation on biological specimens with sufficient water content yielded stress buildup capable of material ejection.[32,33] Following

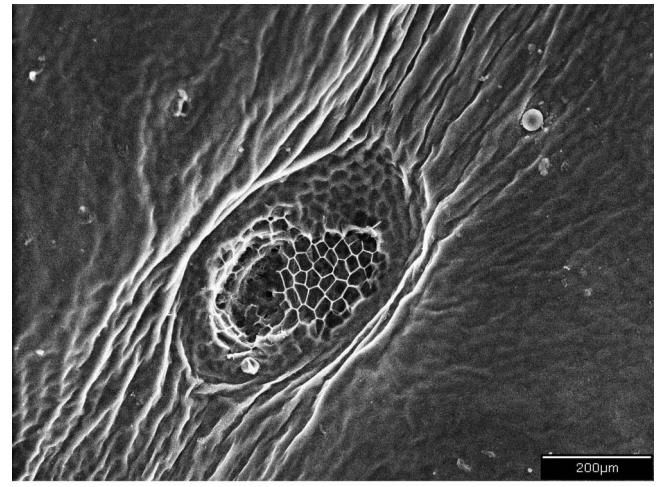

(A)

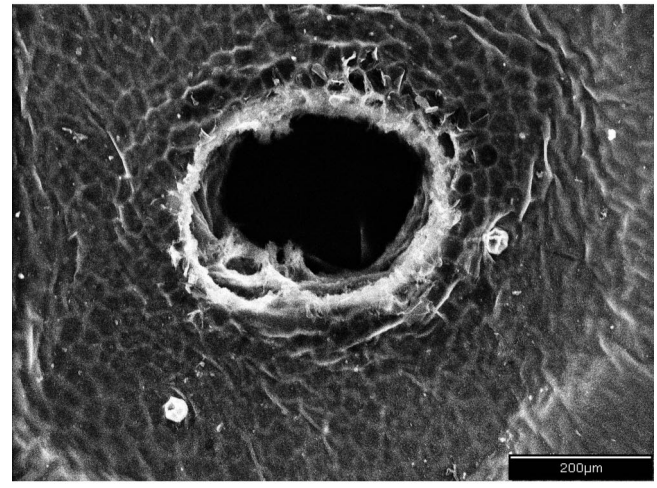

(B)

Figure 1. Scanning electron microscope images of ablation craters produced by (A) a single and (B) 20 laser pulses of ∼2 J/cm^2 fluence, irradiating the adaxial surface of a Zebra plant (*A. squarrosa*) leaf. Scale bars correspond to 200 μm. As a single laser pulse impinged on the leaf surface, the waxy cuticle and some of the upper epidermal and palisade cells were removed from a slightly elliptical area with axes of 300 and 280 μm. Multiple laser pulses penetrated deeper, ablating the palisade and spongy mesophyll cells as well. Eventually the lower epidermal cells and the cuticle were also ablated, resulting in a slightly larger perforation area (350-μm diameter). The wrinkles on the cuticle were caused by the collapse of the underlying cells due to rapid water loss in the vacuum environment during SEM imaging.

exposure to single and multiple laser pulses of 2 J/cm^2 fluence, the ablation craters were characterized with scanning electron microscopy (SEM). The SEM image of the leaf surface taken after a single laser pulse (see Figure 1A) indicated that the upper cuticle, the adaxial epidermal, and some of the palisade mesophyll cells were removed from a slightly elliptical area with axes of 300 and 280 μm. After ∼20 laser pulses in a slightly increased circular area (350-μm diameter), the underlying spongy mesophyll as well as the abaxial epidermal cells and cuticle were also removed and the ∼400-μm-thick leaf was perforated (see Figure 1B).

(32) Venugopalan, V.; Nishioka, N. S.; Mikic, B. B. *Biophys. J.* **1996**, *70*, 2981–2993.

(33) Apitz, I.; Vogel, A. *Appl. Phys. A; Mater. Sci. Processing* **2005**, *81*, 329–338.

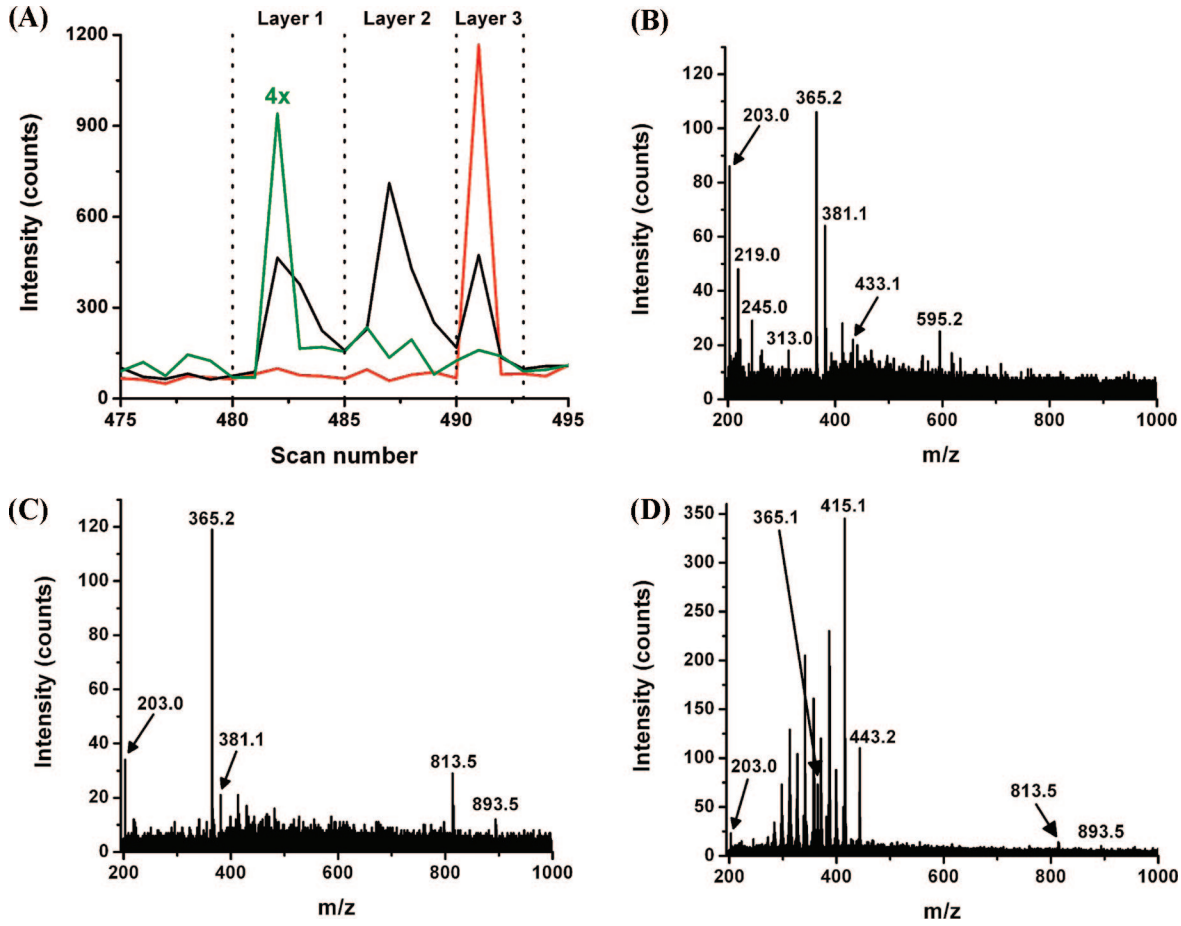

Figure 2. Depth profiling with LAESI-MS. The abaxial cuticle of a Peace lily leaf was marked with a red Sharpie pen and the tissue was ablated from the top by consecutive laser pulses of ~0.2 J/cm^2 fluence. The lower cuticular surface was reached within 3−4 laser shots, enabling us to probe the molecular makeup of ~50−60-μm layers. Panel A shows the ion abundance of potassiated sucrose (black curve), kaempferol, or cyanidin glucoside (olive curve, intensity 4× magnified) and the rhodamine 6G cation (red curve) from the dye component of the red ink. The mass spectrum for layer 1 (see panel B) showed that the adaxial cuticle and epidermal cells were rich in sugars (rhamnose and sucrose) and in kaempferol or cyanidin glycosides. Panel C indicated that the underlying spongy mesophyll section (Layer 2) was of an altered chemical composition. Unidentified ions at *m/z* 813 and 893 were unique for this layer, also rich in sugars. As presented in panel A, the third pulse (layer 3) yielded abundant ion signal for the rhodamine 6G. The corresponding mass spectrum (see panel D) contained ions originating from the dye. These results prove the depth profiling capabilities of LAESI, currently not offered by any ambient ionization method.

Figure 1 shows wrinkles on the cuticular surface surrounding the ablation marks. They are likely the result of the collapse of underlying cells due to dehydration during SEM imaging; the water loss is believed to be caused by the SEM vacuum facilitating the evaporation through the areas ablated by the laser beam.[34] Removal of the protecting waxy cuticle layer through the mid-infrared laser ablation exposes the underlying water-rich cells and makes them more prone to these effects. Consequently, during SEM imaging, the areas adjacent to the ablation undergo considerable tissue deformation. Indeed, wrinkling of the cuticle was only noticed around the ablation marks and the areas where the tissue was cut for SEM mounting purposes. Thus, these structural changes were associated with the vacuum exposure rather than with the laser ablation of the tissue.

The SEM images indicate no significant amount of debris deposited on the leaf surface around the ablated area. As a result, in a LAESI-MS imaging experiment, the adjacent pixels are unlikely to be affected by cross-contamination due to the ablation.

Depth Profiling of Leaf Tissue. The SEM images in Figure 1 suggest that consecutive laser pulses with appropriate energy in a LAESI experiment can be used for depth profiling. This was demonstrated on Peace lily (*S. lynise*) leaves (~200-μm thickness) with laser pulses of ~0.2 J/cm^2 fluence. The tensile strength of these leaves was lower than that of *A. squarrosa*; thus, it required a decreased fluence for successful ablation. To chemically mark the abaxial cuticle, a small amount of dye was deposited on it by a red Sharpie fine point marker. Ablating from the adaxial side, the chemicals in the ink, such as the commonly used red dye rhodamine 6G (*m/z* 443), were detected after 3−4 laser pulses, indicating an ~50−60 μm/pulse average tissue removal rate. Due to the inhomogeneous distribution of water in the various layers, the removal rate, however, may vary. The cuticle and the epidermal cells are known to contain less water than the mesophyll region. Therefore, the first laser pulse is likely to penetrate to a larger depth in comparison to the second one.

Mass-selected ions for sodiated sucrose and rhodamine 6G from *S. lynise* are shown in Figure 2A during the course of LAESI with three consecutive laser pulses. The first ablation (layer 1)

(34) Eveling, D. W. *New Phytol.* **1984**, *96*, 229–237.

yielded abundant sodiated and potassiated sugar ions including rhamnose (m/z 203), and sucrose (m/z 365 and 381) (see Figure 2B). An ion with nominal m/z 595 was also detected at appreciable intensities (signal/noise = 3.8), which could be assigned to kaempferol or cyanidin glucoside rhamnoside (see details in Supporting Information, Table 1). Its presence in layer 1 was in agreement with previous results showing that such glycosides were mainly localized in the upper epidermal layer to protect the leaves by their ultraviolet absorption or by scavenging radicals.[35,36] Indeed, this metabolite was only detected in the top layer of the leaf.[37] The second laser pulse (layer 2; see Figure 2C) yielded additional, yet-unassigned molecular species at nominal m/z 813 and 893 indicating the different molecular makeup of the mesophyll layer. According to the selected ion monitoring results illustrated in Figure 2A, the rhodamine 6G ion was detected after 3−4 laser pulses (layer 3), showing that at that stage the lower cuticle was sampled. Indeed, the corresponding mass spectrum in Figure 2D shows the presence of the related ions. This crude demonstration of depth profiling indicated 50−60 μm axial or depth resolution.

Depth profiling in combination with two-dimensional imaging holds the potential for three-dimensional molecular analysis with LAESI-MS. This imaging mode would enable the mass spectrometric analysis of subsurface features in biological systems.

Altered Metabolism in Variegation Sectors. LAESI analysis on the green and yellow sectors of *A. squarrosa* leaves yielded mass spectra rich in singly and doubly charged ions up to m/z ~1500. Examples of the mass spectra from the green (top panel) and yellow sectors (bottom panel) are shown in Figure 3A. Many of the detected ions were tentatively assigned on the basis of accurate mass measurements, isotope patterns, and collision-activated dissociation experiments in combination with broad plant metabolomic database data (www.arabidopsis.org, http://biocyc.org, http://www.metabolome.jp last accessed on September 30, 2007). Cautious use of these databases is justified as plants often share similar metabolomic features due to evolutionary reasons. A partial list of assignments for the ions detected below m/z 1000 is shown in Supporting Information, Table 1. Certain experimental m/z values are compatible with several assignments as the identification of isomeric species was either impossible or not attempted. Other studies utilizing chiral separation methods, nuclear magnetic resonance, and X-ray spectrometry in combination with mass spectral data, however, have accumulated extensive information on the most abundant plant metabolites. For example, much of the hexose sugars are likely to be found as glucose, as a result of photosynthesis. Therefore, the flavonoid hexosides observed in the mass spectra were assigned as glucosides in Supporting Information, Table 1. Larger ions ($>m/z$ 1000) likely correspond to protonated and sodiated forms of di- and triacylglycerols. Vacuum MALDI-MS experiments have shown the presence of these lipids in plant seeds and fruits in large amounts.[38]

The LAESI mass spectra in the $100 \le m/z \le 300$ range were rich in moderate abundance ions. Although the assignment of these ions was hindered by the interference from the electrospray solvent ions, careful scrutiny revealed them to be acids or other nonaromatic products of the primary plant metabolism. As an example, metabolites in the citric acid cycle, including succinate, fumarate, malate, and citrate/isocitrate, could be identified with a mass accuracy of better than ~25 mDa, despite the increased chemical noise and lower ionic intensities in this mass range (data not shown).

At higher masses, the LAESI mass analysis revealed differences in the metabolism of the green and yellow sectors of the Zebra leaves. For example, kaempferol, luteolin, and their various derivatives were only detected from the yellow sectors. Plant variegation is frequently the result of downregulation or complete loss of photosynthetic cells. These sectors therefore lose their natural green color and appear to be white. Natural dyes (e.g., anthocyanins) can color the white tissues, turning them into red, blue, etc. Indeed, the secondary metabolites with sector specificity in Supporting Information, Table 1, highlighted in light yellow, are often yellow crystallites in their pure form. This would partially explain why the achlorophyllous regions of the Zebra leaves are not white, but have a light yellow tone. The mass spectra often showed ~1.5−5 times more abundant sucrose signal (potassiated and sodiated) from the yellow sectors. This is in good agreement with the known properties of maze variegation. Yellow sectors in these leaves have recently been shown to excessively accumulate starch.[39]

Probably due to the layered structure of the leaves, no metabolites specific to the green area were identified. This was rationalized by a lack of variegation on the abaxial side of the leaf, bearing a uniform green color. Optical microscopy of the leaf cross section also revealed the layered nature of the yellow sectors with underlying green tissue. Thus, during the multishot analysis with LAESI, these green regions were also sampled. Future depth profiling of the yellow sectors, however, may reveal metabolites characteristic to the green layers only.

Several of the identified yellow sector-specific secondary metabolites (see Supporting Information, Table 1) belonged to common biosynthetic pathways. For example, panels B and C in Figure 3 present alternative pathways for kaempferol and luteolin that are consistent with the secondary metabolites detected by LAESI-MS. As kaempferol and luteoline are structural isomers, tandem mass spectra alone do not differentiate between them and between their derivatives. Thus, for every assignment labeled with an asterisk in Figure 3B and C, two possibilities exist. The presence of these secondary metabolites was consistent with results obtained on variegated *tdy1* mutant maze leaves that showed a tendency to accumulate anthocyanins.[39]

Two-Dimensional in Vivo Molecular Imaging on a Leaf. The distribution of metabolites in the green and yellow sectors of *A. squarrosa* was captured by imaging LAESI-MS. The molecular makeup of the leaf in the laser focal volume was probed while moving the target stepwise. To avoid the overlapping of the circular analysis areas (350 μm in diameter), a displacement of 400 μm was used to scan on a two-dimensional grid, over a 4×12

(35) Strack, D.; Pieroth, M.; Scharf, H.; Sharma, V. *Planta* **1985**, *164*, 507–511.
(36) Weissenbock, G.; Hedrich, R.; Sachs, G. *Protoplasma* **1986**, *134*, 141–148.
(37) Osborn, J. M.; Taylor, T. N. *Bot. Gazette* **1990**, *151*, 465–476.
(38) Dreisewerd, K.; Draude, F.; Kruppe, S.; Rohlfing, A.; Berkenkamp, S.; Pohlentz, G. *Anal. Chem.* **2007**, *79*, 4514–4520.
(39) Braun, D. M.; Ma, Y.; Inada, N.; Muszynski, M. G.; Baker, R. F. *Plant Physiol.* **2006**, *142*, 1511–1522.

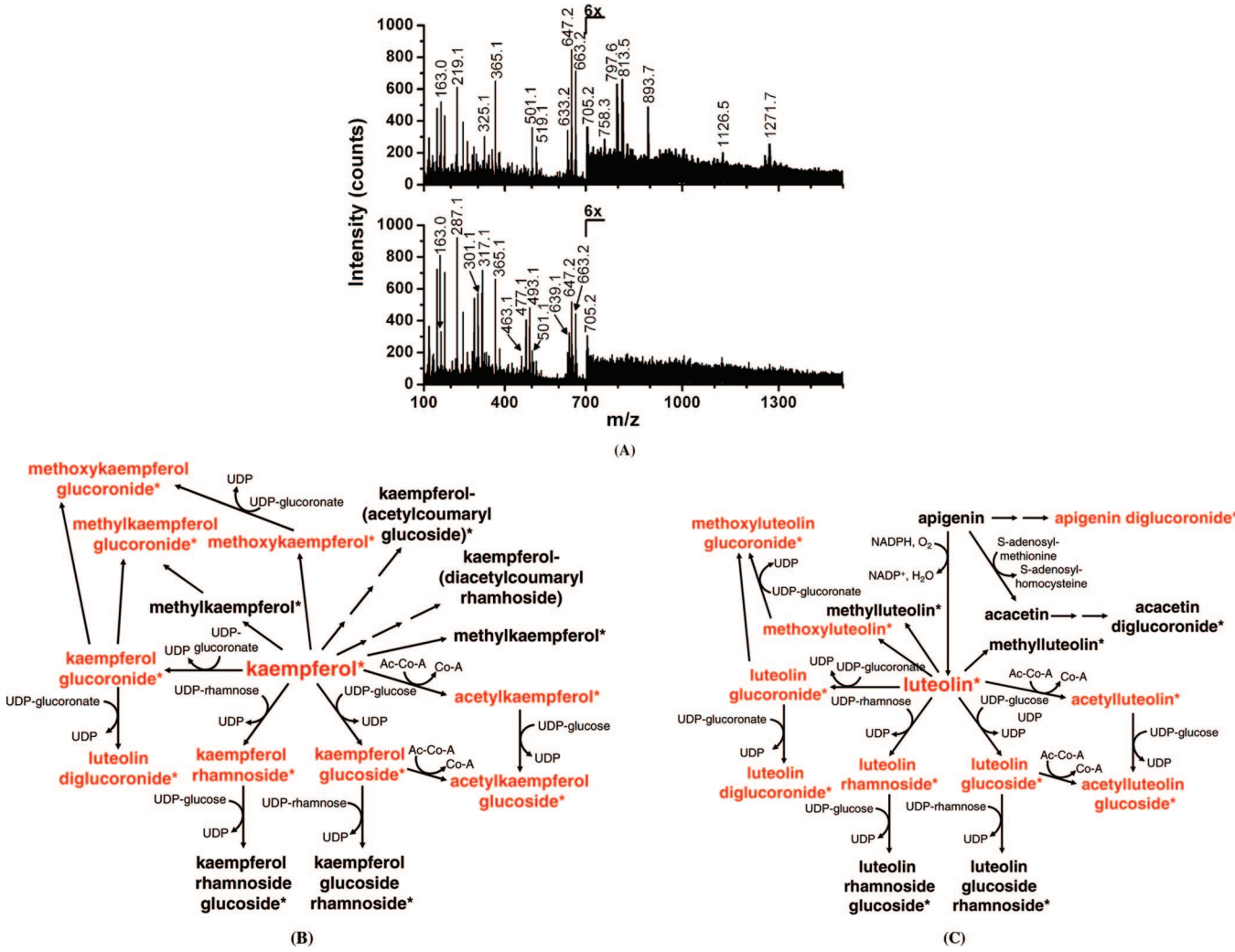

Figure 3. LAESI mass spectrometric analysis on the green (top spectrum in panel A) and yellow sectors (bottom spectrum in panel A) of live variegated *A. squarrosa* leaves showing differences in chemical composition. For example, some secondary metabolites such as kaempferol or luteolin (see Supporting Information, Table 1) were only found in the achlorophyllous regions. Optical microscopy of the leaf cross section revealed the layered nature of the yellow sectors with underlying green tissue. By monitoring the spatial distribution of metabolites and their derivatives in the leaf, specific biosynthetic pathways could be followed. Panels B and C present alternative pathways for kaempferol and luteolin consistent with the secondary metabolites detected by LAESI-MS. As kaempferol and luteoline are structural isomers, tandem mass spectra alone often do not differentiate between them and between their derivatives. Thus, for every assignment labeled with an asterisk, two possibilities exist. Metabolites detected only in the yellow regions are in color. These results suggested that the biosynthesis of some secondary metabolites was either localized in the yellow variegated areas only, or metabolite accumulation from the wild-type tissues took place due to transport.

mm^2 area yielding a total of 363 pixels. At each of the analysis points as the focused mid-IR beam impinged on the surface, ions were registered at up to 3000 counts/s rate by the mass spectrometer. The ion intensities then quickly decayed reaching noise level within 2−3 s (20−30 laser shots), indicating complete local removal of the tissue (i.e., the perforation of the leaf).

Molecular images were constructed by correlating the peak areas observed during mass-selected ion monitoring to the absolute coordinates of the analyzed point at the time (see Figure 4). Examples for the distribution of the m/z 663, 493, and 813 ions are provided as color-coded contour plots in panels C−E of Figure 4, respectively. The molecular image for kaempferol(di-acetylcoumaryl rhamnoside), see Figure 4C, revealed a uniform distribution over the analyzed area of the leaf. The presence of methoxykaempferol glucoronide (Figure 4D), however, was only detected with appreciable abundance in certain sectors. Indeed, these sectors correlated well with the optical image of the variegation pattern (Figure 4A and B). Accumulation of these secondary metabolites in the yellow sectors would not explain their complete absence (signal/noise <3) in the green areas. Thus, methoxykaempferol glucoronide and the related metabolites depicted in Figure 3A appear to be produced in biosynthetic processes selectively operating in the yellow sectors.

The ion m/z 813, yet unassigned, was often detected at an increased intensity in the green regions of the leaf. Indeed, comparing Figure 4E and D reveals that the distributions of m/z 813 and 493 are anticorrelated. As mentioned above, the yellow sectors of the leaf were composed of a yellow top layer with a thin underlying layer of green tissue. Therefore, m/z 813 can be perceived as unique for the chlorophyllous tissue. Depth profiling of the m/z 813 distribution could provide further evidence for this hypothesis. Ions detected at higher m/z values, such as m/z 743, 745, 747, 758, 894, etc., (data not shown), seem to follow a similar

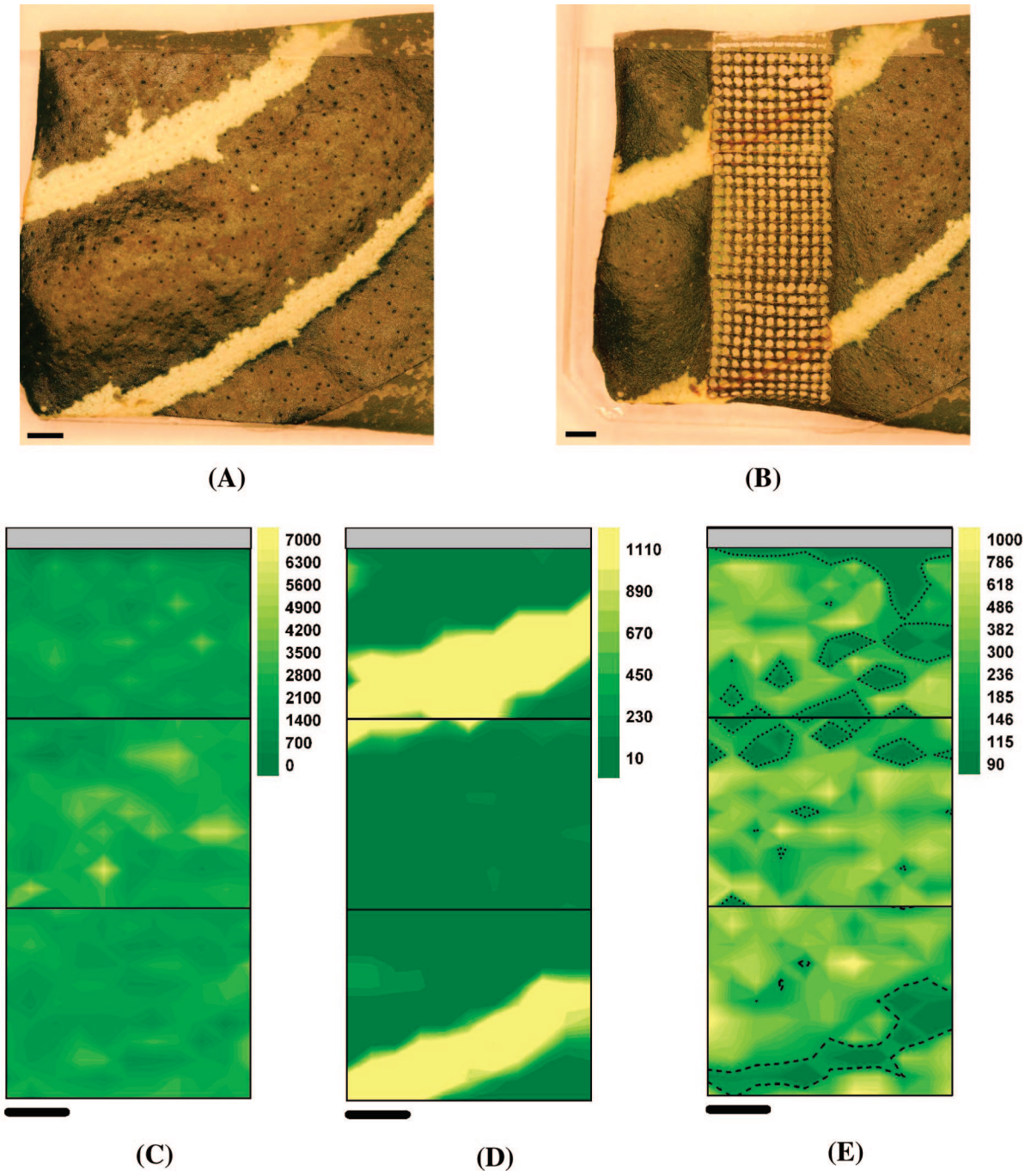

Figure 4. Molecular composition of the variegated *A. squarrosa* leaf (A). The leaf was probed with LAESI-MS while rastering the surface with a focused infrared laser beam over three adjacent 4 mm by 4 mm areas. The live tissue surface was ablated at a circular area (350-μm diameter) with a 400-μm step size (see inset B). Contour plots C−E show the distribution of ions detected at *m*/*z* 663, 493, and 813, respectively. Kaempferol-(diacetyl coumaryl-rhamnoside), assigned to *m*/*z* 663, was detected in both the yellow and the green sectors of the leaf and showed a uniform distribution in intensity. Methoxykaempferol glucoronide (*m*/*z* 493) was only present in the variegated areas and established a molecular distribution that was in good agreement with the pattern of the yellow sectors, shown in the optical images before and after the analysis (see insets A and B). The yet-unassigned ion at *m*/*z* 813 usually occurred at higher abundances in the nonvariegated areas. Black dotted contour lines highlight the distribution of this species at a total intensity level of 164 in inset E. Note that these sectors appear to be in an inverted relationship with those for *m*/*z* 493. Intensity bars represent chromatographic areas for a mass-selected ion. Length scale bars correspond to 1 mm. These results also demonstrate that imaging LAESI-MS does not suffer from redistribution of analytes. The lateral resolution appears to be limited by the focal spot size, offering great advances in imaging of biochemical changes on a molecular level.

pattern. Although not assigned, these species are likely to be products of lipid biosynthesis.

Comparing the optical images before (Figure 4A) and after (Figure 4B) LAESI imaging revealed that analyte redistribution did not affect nearby pixels. This was also anticipated from the SEM characterization of the ablation craters (Figure 1) that indicated no appreciable redeposition of the ablated tissue material on the surface. An important feature of imaging LAESI is that the lateral resolution is limited by the focal spot size of the ablating laser beam. At its current state, the spatial resolution of LAESI in molecular imaging

experiments is estimated to be 200−300 μm (data not shown). LAESI has the potential to significantly improve this by using tighter focusing of the laser beam. Application of an aspherical reflective objective is being explored, and preliminary results indicate 20−50-μm focal spots. Ablation and analyte detection on this length scale promises to open the way to perform panoramic molecular analysis on a single-cell level with LAESI-MS.

CONCLUSIONS

In this study, we demonstrated the lateral mapping of metabolite distributions and their variations with depth on plant leaves with LAESI-MS. With over 40 primary and secondary metabolites detected (36 of them assigned), LAESI imaging presents a useful combination of panoramic analysis with an imaging method of moderate spatial resolution. Although at this stage in terms of spatial resolution LAESI cannot compete with vacuum imaging methods such as SIMS, MALDI,[40] and graphite-assisted laser desorption/ionization[41,42] imaging, its ability to work with live specimens without sample preparation enables unique applications and opens new directions in biochemical research.

The efficacy of LAESI imaging to diverse biological tissues primarily depends on the homogeneity of their water content and tensile strength. For example, due to the lower water content, wood formation or calcification of soft tissue results in decreased efficiency of coupling the laser energy into the sample. Large differences in tensile strength (e.g., between tendon and muscle) can alter the nature and propensity of material ejection through laser ablation. Nevertheless, moderate changes in these properties can be compensated by altering the laser pulse energy, the wavelength, or both. For example, working at 6.1 and 6.45 μm, the amide I and II absorption regions, respectively, enabled the efficient ablation of cartilage.[43]

Focusing of the mid-IR laser beam in our experiments is limited by the optical arrangement to ~350 μm. We demonstrated that this enables a ~350-μm spatial resolution while avoiding the overlap of adjacent analysis areas during LAESI imaging. Improving the spatial resolution of LAESI imaging requires positioning the sample with an increment smaller than the dimension of the ablation crater. This technique, known as oversampling, has recently proved useful under atmospheric pressure conditions in infrared MALDI imaging.[11] Alternatively, tighter focusing of the laser beam can offer similar enhancements while simultaneously maintaining the sensitivity of mass spectrometric analysis. Although mid-IR laser ablation with an aspherical lens has already been demonstrated to produce ~50-μm ablation marks on a leaf sample, the detection of the ions produced through LAESI requires further work. Ultimately the successful combination of lateral imaging with depth profiling at improved spatial resolution promises three-dimensional imaging of metabolite and xenobiotics distributions from biological tissues.

(40) Shroff, R.; Vergara, F.; Muck, A.; Svatos, A.; Gershenzon, J. *Proc. Natl. Acad. Sci. U. S. A.* **2008**, *105*, 6196–6201.
(41) Zhang, H.; Cha, S. W.; Yeung, E. S. *Anal. Chem.* **2007**, *79*, 6575–6584.
(42) Cha, S. W.; Yeung, E. S. *Anal. Chem.* **2007**, *79*, 2373–2385.
(43) Youn, J. I.; Sweet, P.; Peavy, G. M.; Venugopalan, V. *Lasers Surg. Med.* **2006**, *38*, 218–228.

ACKNOWLEDGMENT

This work was supported by the National Science Foundation under grant 0719232, by the Department of Energy (DEFG02-01ER15129) and by the W. M. Keck Foundation (041904). Any opinions, findings, and conclusions or recommendations expressed in this material are those of the authors and do not necessarily reflect the views of the supporting organizations. The authors thank Jessica A. Stolee (George Washington University) for the kind help provided with the SEM imaging in this study.

SUPPORTING INFORMATION AVAILABLE

Table of secondary and some primary metabolites tentatively assigned on the basis of accurate mass messurements, isotope patterns, and CID of selected ions in conjunction with plant metabolomic database searches. This material is available free of charge via the Internet at http://pubs.acs.org.

Received for review February 27, 2008. Accepted April 21, 2008.

AC8004082